Available online at www.sciencedirect.com
ScienceDirect
Journal of Sound and Vibration 319 (2009) 140–162
JOURNAL OF SOUND AND VIBRATION
www.elsevier.com/locate/jsvi

Robust estimation of excitations in mechanical systems using M-estimators—Experimental applications

Paolo Pennacchi*

Dipartimento di Meccanica, Politecnico di Milano, Via La Masa 34, I-20156 Milano, Italy

Received 21 August 2007; received in revised form 7 May 2008; accepted 12 May 2008
Handling Editor: M.P. Cartmell
Available online 25 June 2008

Abstract

This second part of the study presents some experimental applications to mechanical systems in which the results of excitation estimation, obtained using traditional least squares and M-estimate, are compared.

The first case presented is a single input–multiple outputs system: a simple test-rig for the study of the vibrations of a two-degrees of freedom system is employed to identify the constraint displacement that causes the measured mass vibrations in presence of heavy noise.

The second case is a multiple inputs–multiple outputs system: a rotor test-rig is used to identify the positions, the amplitudes and the phases of two unbalances using the vibrations measured in the bearings. In this case, also an additional theoretical part is introduced about the basics of model-based identification in the frequency domain applied to rotor dynamics.

The last case is again a single input–multiple outputs system, but in an industrial application: experimental vibrations of a 320 MW steam turbo-generator are used to identify position and amount of a known balancing mass in an on-field real case.

Moreover, whilst in the numerical examples presented in the first part the knowledge of the system was perfect, in these cases some uncertainties are present also in the system model.

Finally, the paper introduces the use of the M-estimate technique to evaluate the adequacy the model of the system, by means of the analysis of the weights attributed to the measures as a function of the frequency of the excitation.

1. Introduction

The theory of M-estimators, applied to the robust identification of mechanical systems, has been introduced in the first part of the study [1]. Since several types of M-estimators actually exist, their advantages and drawbacks have been highlighted by means of numerical examples and the types more suitable for mechanical systems have been proposed.

In this second part, some experimental results are presented in order to further validate the proposed method. Contrarily to what has been done in the numerical cases, in which the knowledge of the system model,

*Tel.: +39 2 23 99 8440; fax: +39 2 23 99 8492.
E-mail address: paolo.pennacchi@polimi.it

0022-460X/$ - see front matter © 2008 Elsevier Ltd. All rights reserved.
doi:10.1016/j.jsv.2008.05.017

or of its parameters, was always perfect and noise was present only (deliberately) on the outputs, in these experimental cases the uncertainties are not only in the outputs but also in the system model.

In particular, the noise on the outputs is that typical of actual measuring systems and is neither known *a priori* nor its evaluation is performed. In a case, nothing is even done to avoid the presence of easily eliminable noise. As it regards the model, it is deliberately approximate in the first case, in which the dynamic response of the supporting structure is totally and deliberately neglected. In the other cases related to rotor dynamics, there are some ranges of frequency in which the model is not reliable due to the stiffness and damping coefficients of the journal bearings that are linearized and calculated for some rotating speeds only.

The first example presented here is a simple single input–multiple outputs (SIMO) system: a test-rig for the study of the vibrations of a two-degrees of freedom (dofs) system. Two masses are linked to a horizontal guide by means of rollers and connected by springs. The displacement of a constraint excites the vibration of the system. In this case, the supporting structure has a natural frequency very close to one of the natural frequencies of the system. This fact is intentionally neglected in the model, in which the supporting structure is considered rigid. Besides the measurement chain is not shielded and filters are not used.

In the second example, the M-estimators are used to evaluate the value and the position of two unbalances in a rotor-dynamics test-rig, starting from the vibrations measured in the bearings. The increase of accuracy is shown in comparison to results obtained using the traditional least squares. This system is of multiple inputs–multiple outputs (MIMO) type. In this case, since it is also necessary to evaluate the position of the excitations along the shaft line, it is necessary to implement the algorithm of the iterated reweighed least squares (IRLS) in the model-based identification method proposed in Ref. [2]. Therefore, the necessary theory is shortly introduced. Given that it is necessary to insert the stiffness and the damping coefficients of the journal bearings in the rotor model, these last ones are linearized according to the standard methods of the rotor dynamics [3–5]. Anyway the coefficient calculations could not be accurate in some rotating speed ranges. In particular, it is shown that the knowledge of the weights attributed by the IRLS algorithm to the various measures can also be used to assess the adequacy of the model.

The last example is related to the robust identification of a balancing mass in a 320 MW steam turbo-generator. In this case the system is again of SIMO type and it is necessary to also estimate the position of the unbalance along the shaft train, similar to the previous MIMO system. Being an on-field application, a remarkable noise is present in the measurement chain and there are several uncertainties in the model, not only in the bearing coefficients but also in the dynamical behaviour of the machine supporting structure. The results obtained using the M-estimate are compared with those of least squares.

2. Experimental results for a SIMO system: 2 dofs mass–spring–damper system

In order to have a more meaningful evaluation of the performances of the M-estimators in mechanical systems, a simple experimental set-up has been used to perform identification of the excitation in a real environment, in which intentionally no care has been taken to avoid corruption of the measures. Moreover, the knowledge of the system is not perfect.

The experimental set-up is shown in Fig. 1. The system is excited by the displacement of the constraint on the left side, which is driven by means of a ball screw and an asynchronous motor actuated by an inverter. Two masses, one connected to the other and to the constraints with linear springs, move on linear motion guides over rollers.

The motor can drive the constraint in order to have a harmonic displacement with constant amplitude at a given frequency. The damping of the system is modelled by means of lumped linear dampers in parallel to the springs. The scheme of the system is shown in Fig. 2.

The equations of motion of the system are

$$\begin{bmatrix} m_1 & 0 \\ 0 & m_2 \end{bmatrix} \begin{Bmatrix} \ddot{x}_1 \\ \ddot{x}_2 \end{Bmatrix} + \begin{bmatrix} c_1 + c_2 & -c_2 \\ -c_2 & c_2 + c_3 \end{bmatrix} \begin{Bmatrix} \dot{x}_1 \\ \dot{x}_2 \end{Bmatrix} + \begin{bmatrix} k_1 + k_2 & -k_2 \\ -k_2 & k_2 + k_3 \end{bmatrix} \begin{Bmatrix} x_1 \\ x_2 \end{Bmatrix} = \begin{Bmatrix} k_1 y_0 + c_1 \dot{y}_0 \\ 0 \end{Bmatrix}. \quad (1)$$

The friction between the rollers and the guide is taken into account by means of the equivalent damping coefficients in Eq. (1). As can be noticed from Fig. 1, the vibrating system is not installed on a rigid support,

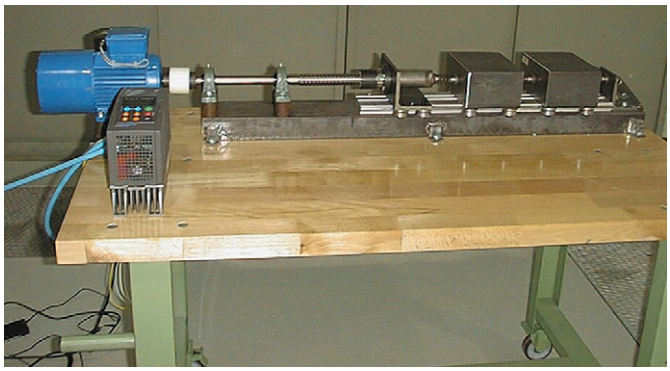

Fig. 1. Experimental test-rig.

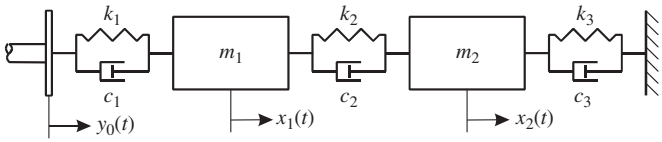

Fig. 2. Model of the system.

which is instead implicitly assumed in Fig. 2 and Eq. (1), but on a table, the stiffness and damping of which are unknown. These aspects are actually model uncertainties.

The masses and the left constraint are equipped by an accelerometer each. The displacements of the masses correspond to the considered dofs of the system, while that of the constraint is acquired in order to check the correspondence of the amplitude to the displacement imposed value by the inverter. A further confirmation about the constraint displacement is given by a linear variable differential transformer (LVDT).

Complex algebra is used later on. Since the constraint displacement is harmonic: $y_0 = Y_0 e^{i\varphi} e^{i\Omega t}$, also the steady-state displacements of the masses are harmonic. The steady-state solution is obtained solving

$$(-\Omega^2\mathbf{M} + i\Omega\mathbf{C} + \mathbf{K})\mathbf{X} = \begin{Bmatrix} i\Omega c_1 + k_1 \\ 0 \end{Bmatrix} Y_0 e^{i\varphi} \tag{2}$$

and finally:

$$\mathbf{X} = (-\Omega^2\mathbf{M} + i\Omega\mathbf{C} + \mathbf{K})^{-1} \begin{Bmatrix} i\Omega c_1 + k_1 \\ 0 \end{Bmatrix} Y_0 e^{i\varphi}. \tag{3}$$

The least squares (L_2) and the M-estimators described in the first part of the paper have been used to estimate the amplitude and the phase of the left constraint displacement, which has been applied with a nominal value of $Y_0 = 1.8$ mm and $\varphi = 0^\circ$.

The model parameters have been identified before executing the tests. Static tests allowed to measure the mass values ($m_1 = m_2 = m = 23.5$ kg) and the spring stiffness ($k_1 = k_2 = k_3 = k = 5740$ N/m). The equivalent damping coefficients have been evaluated by means of experimental modal analysis and are $c_1 = c_3 = 34.31$ Ns/m, $c_2 = 3.98$ Ns/m.

The experimental tests have been performed by forcing the system in the frequency range between 1 and 5 Hz with a step of 0.25 Hz. The LVDT and the accelerometer on the constraint indicated that the displacement was actually 1.8 mm in average in this frequency range. Once the system reached the steady-state response, the mass accelerations were measured with a sampling rate of 100 sample/s for 20 s of acquisition time. The acquired time histories are affected by heavy disturbances, either electrical or mechanical, which also corrupt the related spectra, since filters are not intentionally used. As an example, the time history of the measured acceleration of the second mass relative to the constraint displacement at 2.25 Hz is presented in

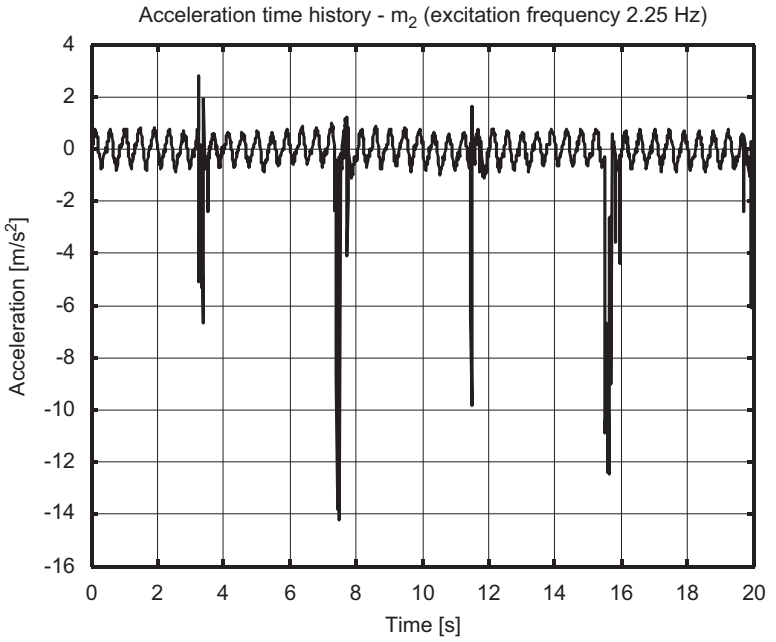

Fig. 3. Time history of the acceleration of mass m_2 with excitation frequency of 2.25 Hz.

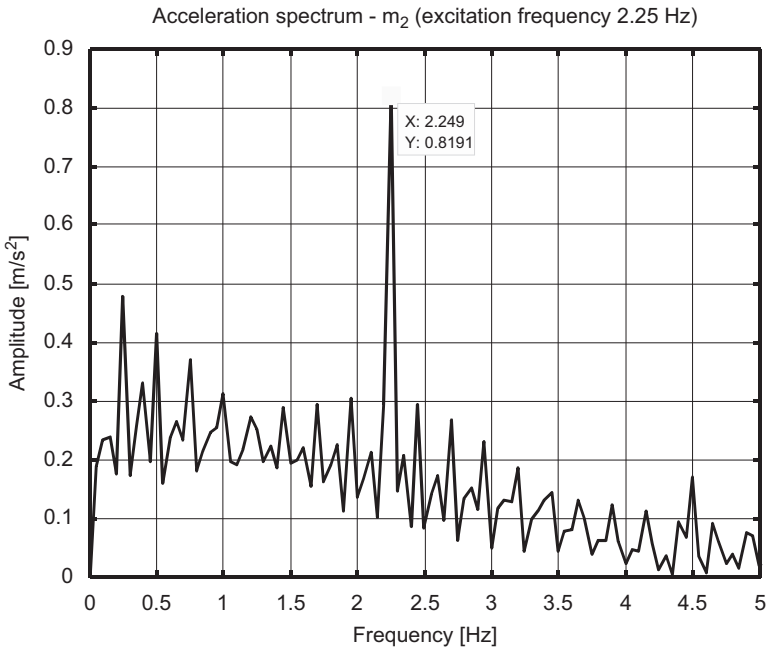

Fig. 4. Spectrum of the acceleration of mass m_2 with excitation frequency of 2.25 Hz.

Fig. 3 along with its amplitude spectrum in Fig. 4. The sinusoidal single frequency component is identified taking the highest peak of the signal spectrum and the corresponding phase.

The experimental frequency response functions have been evaluated automatically considering, for each excitation frequency, the highest peak in the measured spectra. It is important to stress again that this rough method has been chosen in order to test M-estimator performances and to reproduce the worst real-world

condition where not only the amplitude and the phase of the input force but often also its frequency are unknown. If this last piece of information was known, a clever data analysis could be conducted for instance not only using the highest peak but also limiting the peak search in a frequency range close to that of the input.

Fig. 5 shows the comparison between the nominal (solid and dotted lines), given by the model, and the experimental responses of the test-rig (markers only). The difference in the response close to the first resonance of the system (model eigenvalues are equal to 2.4849 and 4.3062 Hz) is particularly evident and is caused by the fact that in this case the supporting structure vibrates strongly. Also close to the second resonance of the system a certain difference is evident, while the responses are sufficiently comparable in the remaining frequency range.

The results obtained by the L_2 and the different types of M-estimators are reported in Table 1. The maximum number of iterations of the IRLS algorithm is fixed at 100 and the stop condition is that in the first

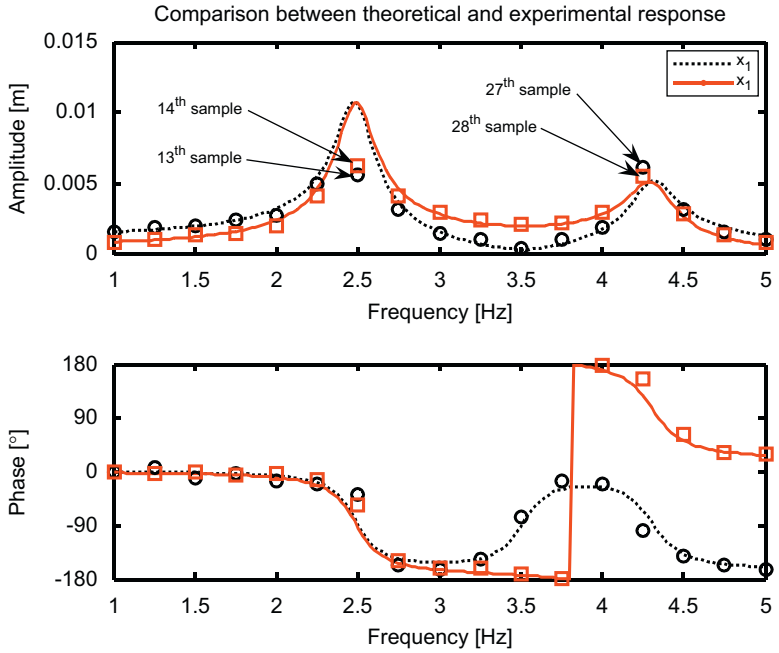

Fig. 5. Comparison between the model and the experimental responses of the test-rig.

Table 1
Identification results

Estimator	Y_0 (mm)	φ (deg.)	Iterations
L_2 (least squares)	1.542	4.4231	
L_1 (least absolute)	1.8253	0.20088	10
L_1-L_2	1.7686	1.9376	20
L_p, $v = 1.2$ (least powers)	1.8127	0.65892	7
Fair	1.7567	1.9498	100
Huber	1.8093	1.6642	17
Modified Huber	1.784	1.6436	100
Cauchy	1.6706	2.6877	100
German-McClure	1.8266	0.51545	100
Welsch	1.5833	3.3767	100
Tukey	1.604	3.3146	100

part of the study, i.e.:

$$\max\left(\begin{array}{l}\left|(\mathrm{Re}(\mathbf{Y}_0^{(t-1)})-\mathrm{Re}(\mathbf{Y}_0^{(t)}))\Big/\mathrm{Re}(\mathbf{Y}_0^{(t-1)})\right|\\ \left|(\mathrm{Im}(\mathbf{Y}_0^{(t-1)})-\mathrm{Im}(\mathbf{Y}_0^{(t)}))\Big/\mathrm{Im}(\mathbf{Y}_0^{(t-1)})\right|\end{array}\right)<1\mathrm{e}-4. \tag{4}$$

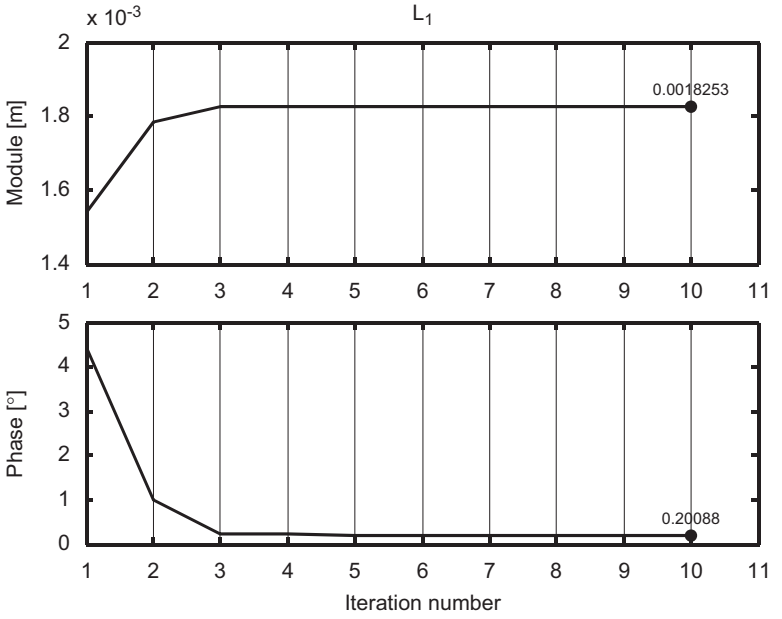

Fig. 6. Estimated values vs. iteration for the L_1-estimate.

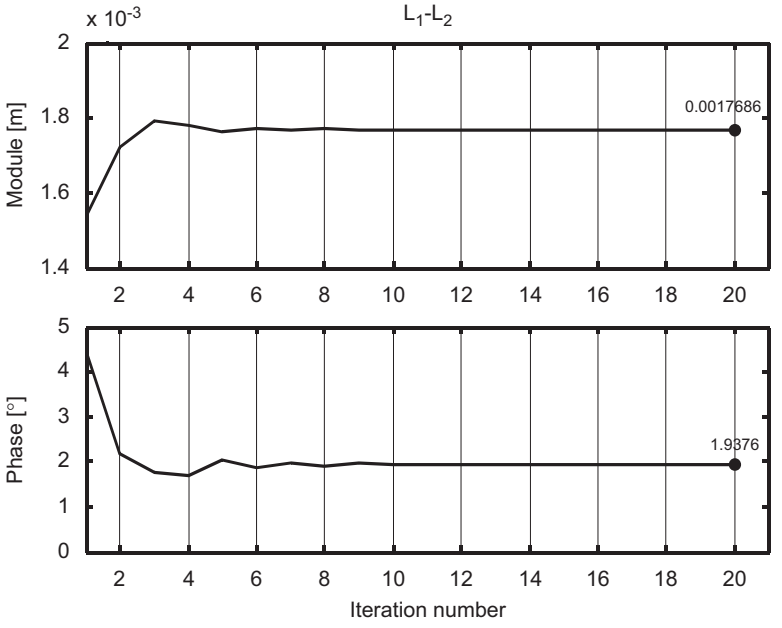

Fig. 7. Estimated values vs. iteration for the L_1-L_2-estimate.

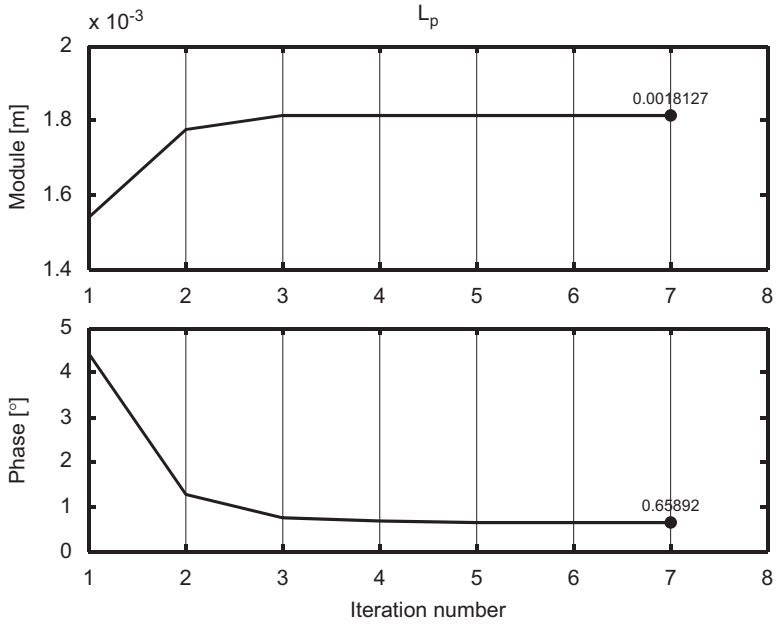

Fig. 8. Estimated values vs. iteration for the L_p-estimate.

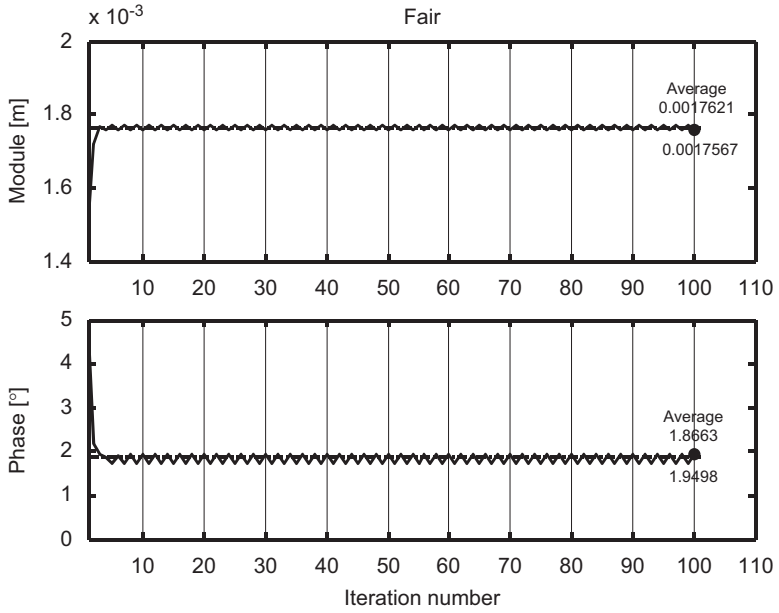

Fig. 9. Estimated values vs. iteration for the Fair estimate.

Figs. 6–15 present the evolution of the excitation estimate as a function of the number of iteration for all the M-estimators adopted. The results obtained indicate that the L_2-estimate is heavily influenced by the disturbances on the measures and by the model inaccuracies: the exciting displacement is not identified correctly. Among the different types of M-estimators, those that do not have a unique solution [6], i.e. Cauchy, German-McClure, Welsch and Tukey, behave badly and the algorithm stops without having reached convergence. Apparently German-McClure gives a good estimate, but this is due to the fact that this value corresponds to the 100th iteration, average value of the estimate is less good (Fig. 13). Also Modified Huber

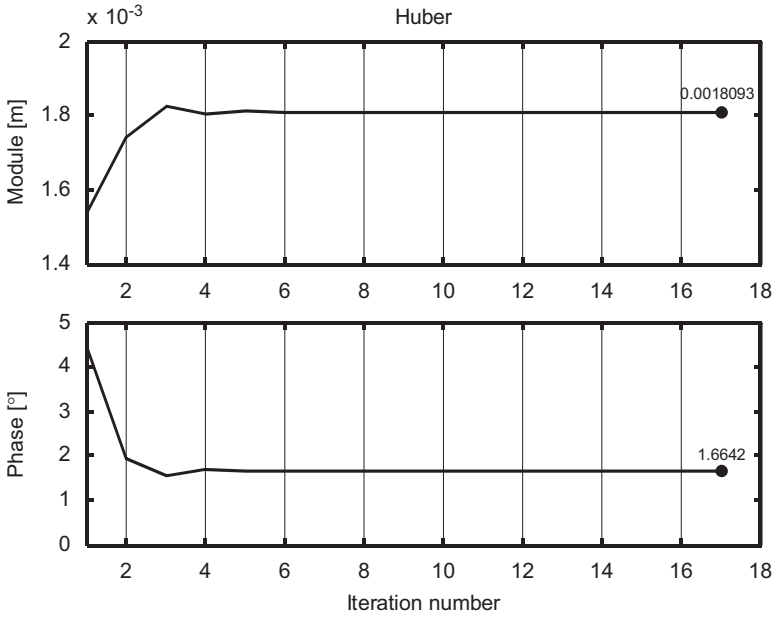

Fig. 10. Estimated values vs. iteration for Huber's estimate.

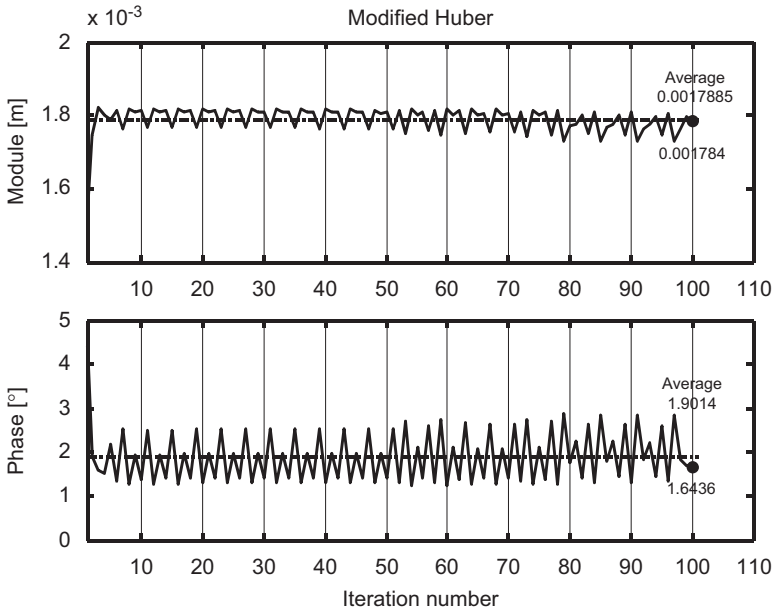

Fig. 11. Estimated values vs. iteration for Modified Huber's estimate.

does not converge even if the estimate is better than the others not converging. L_1 and L_p converge very quickly (Figs. 6 and 8), with a good estimation on excitation module and phase. Huber gives a good estimation and has the advantage of avoiding the numerical instability that could affect L_1 (see Ref. [1], Section 3.1.1) or the v value selection of L_p. In this case, M-estimators having a unique solution are able to give a good estimation of the unknown parameter, even in the presence of disturbances in the experimental response and of inaccuracies in the model.

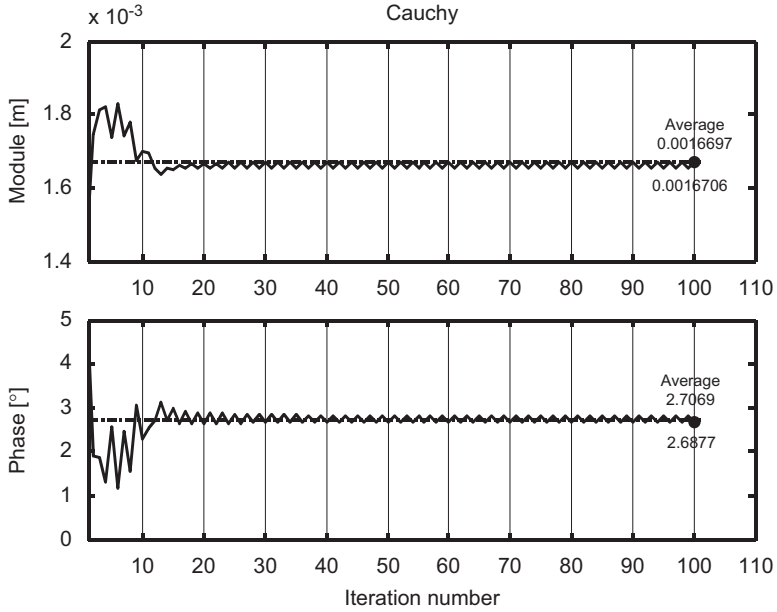

Fig. 12. Estimated values vs. iteration for Cauchy's estimate.

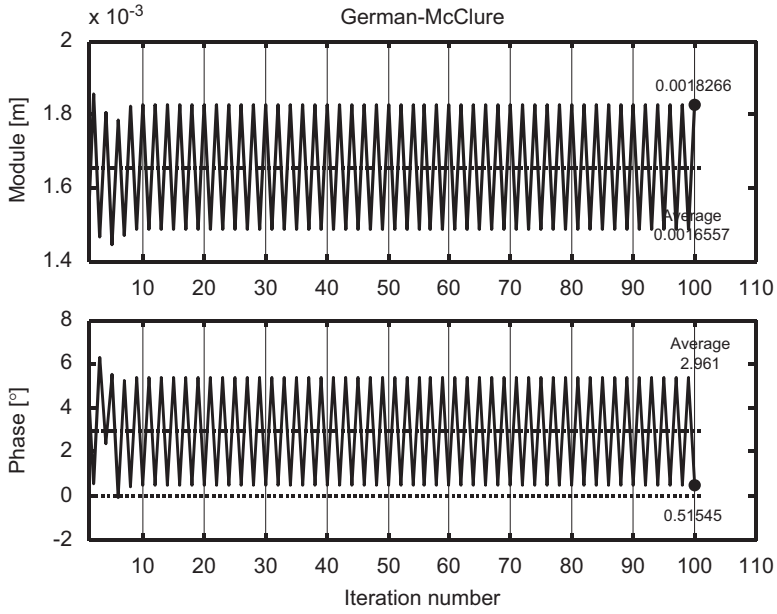

Fig. 13. Estimated values vs. iteration for German-McClure's estimate.

In the following, only Huber's estimator will be used, giving a good compromise between accuracy, relative immunity from numerical instability (see Ref. [1], Section 3.2), independence from arbitrary selections of least power v value and quickness of convergence.

Once again the analysis of the weights attributed to the single samples allows understanding the way of operating of the M-estimate inside the IRLS algorithm. Fig. 16 shows that the weights automatically attributed in the last iteration to the experimental observations that are more influenced by disturbances are very small.

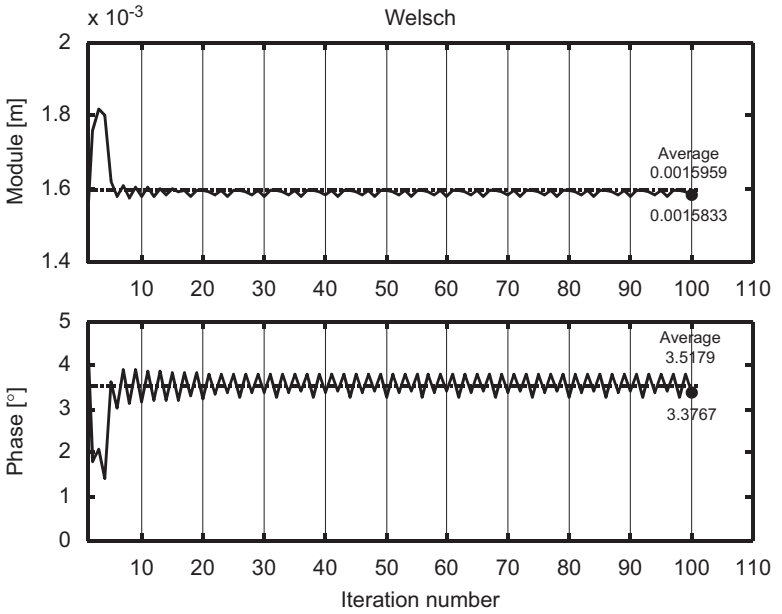

Fig. 14. Estimated values vs. iteration for Welsch's estimate.

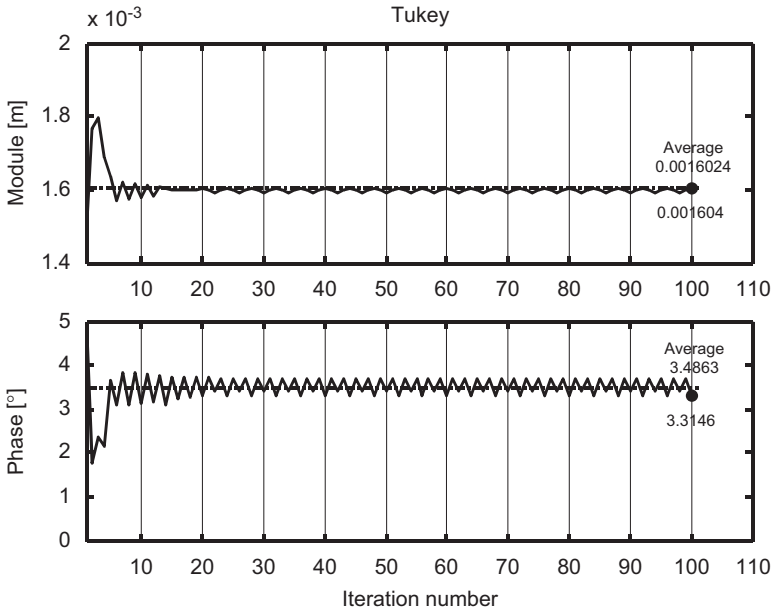

Fig. 15. Estimated values vs. iteration for Tukey's estimate.

3. Experimental results for a MIMO system: identification of two unbalances in a rotor test-rig

3.1. Implementation of M-estimate in rotor systems

In this example, the proposed technique is used to improve the accuracy of fault identification in a rotor test-rig. Practically, the model-based method presented in Ref. [2] is here improved by using the M-estimate instead of the traditional least squares. Since in this case it is also of fundamental importance to locate the

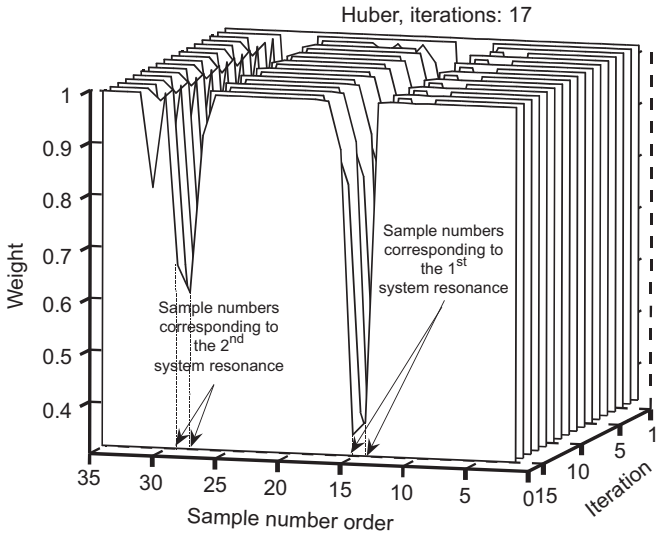

Fig. 16. Weights as a function of the sample number and iterations for Huber's estimate.

excitation (the unbalances) along the rotor shaft, a short introduction to the model-based identification in the rotor system is required.

Model-based identification of faults in rotor systems [7] is essentially a MIMO inverse problem. Some examples have been presented in the time domain [8], but since many types of faults of rotating machinery effect few harmonic components (as well known in the literature starting from Sohre's chart), the harmonic balance approach is preferable. The method is fully described in Ref. [9] and requires the assembling of the complete model of the machine composed by the rotor, the bearings and the supporting structure. The rotor is modelled by means of finite beam elements with 4 dofs per node, whilst the bearing by means of linearized dynamic stiffness coefficients, see, respectively, Refs. [10,11] and [3] for details. The supporting structure can be considered rigid or, more accurately, modelled by means of pedestals or modal representation (see Refs. [9,12–16]). Also *common faults* in rotor dynamics can be modelled by means of *equivalent excitation systems* [9,17]; therefore these terms are considered as synonymous. With regard to the experimental data, *additional vibrations* are used. They are obtained by means of the vector difference of the vibrations in the faulty condition and in a reference condition. Under the hypothesis of linearity of the system, which is satisfied in many cases of common faults in rotating machinery, the additional vibrations are caused by the developing faults only. Further discussion about this topic can be found in Refs. [18,19].

Once the machine has been modelled, the following equations are obtained for each harmonic component, in which the equivalent excitation vector $\mathbf{F}_{f_n}$ has to be identified:

$$[-(n\Omega)^2[\mathbf{M}] + \mathrm{i}n\Omega[\mathbf{C}(\Omega)] + [\mathbf{K}]]\mathbf{X}_n = \mathbf{F}_{f_n}, \tag{5}$$

where $[\mathbf{M}]$ is the mass matrix, $[\mathbf{C}(\Omega)]$ is the complete damping matrix that includes also the gyroscopic matrix calculated at the operating speed, and $[\mathbf{K}]$ is the stiffness matrix.

Because the system is considered as linear, the effect of m faults developing simultaneously can be considered by means of the superposition of the effects for each harmonic component:

$$\mathbf{F}_{f_n} = \sum_{i=1}^{m} \mathbf{F}_{f_n}^{(i)}. \tag{6}$$

These excitations are the multiple inputs (MI) of the system. Moreover, the kth fault acts on few dofs of the system; therefore the vector $\mathbf{F}_{f_n}^{(k)}$ is not a full-element vector, which is convenient to be represented by means of

$$\mathbf{F}_{f_n}^{(k)} = \{\mathbf{L}^{(k)}\}\theta^{(k)}(\Omega), \quad \theta^{(k)}(\Omega) \in \mathbb{C}, \tag{7}$$

where $\{\mathbf{L}^{(k)}\}$ is the localization vector that has all null-elements, except for the dofs to which the exciting system is applied, and $\theta^{(k)}(\Omega)$ is a complex number representing the amplitude and the phase of the fault. Obviously, as many nodes are used for the model, as much the location of the fault is accurate.

In the paper, in which unbalances are going to be identified, it is sufficient to consider the synchronous ($1\times$ rev.) component of the vibration, but the method can be easily modified for other fault types, by using the corresponding fault model and the pertinent harmonics. Since the unbalance can be only applied on the rotor nodes and not on the foundation, the kth unbalance can be expressed as

$$\mathbf{F}_{f_1}^{(k)} = \left\{ 0 \ \vdots \ \underbrace{1 \ \ 0 \ \ i \ \ 0}_{j\text{th rotor node}} \ \vdots \ 0 \ \ \underbrace{0 \ \cdots \ 0}_{\text{foundation dofs}} \right\}^{\mathrm{T}} (mr)^{(k)}\Omega^2 \mathrm{e}^{\mathrm{i}\varphi^{(k)}} = \Omega^2\{\mathbf{L}^{(k)}\}\theta^{(k)}. \tag{8}$$

In Eq. (8) the only elements different from zero are those relative to the horizontal and vertical dofs of the node jth, where the unbalance is supposed to be applied (Fig. 17). Note that the application node is not known *a priori*.

In general, the monitoring data used to identify the fault are collected for many rotating speeds and on different measuring sections, usually referred to as *measuring planes* (which often are corresponding or close to the bearings). The rotating speeds, at which the additional vibrations are available, are organized as a vector of n_p elements:

$$\mathbf{\Omega} = \left\{ \Omega_1 \quad \Omega_2 \quad \dots \quad \Omega_{n_p} \right\}^{\mathrm{T}}. \tag{9}$$

If the measuring planes are l, the experimental vibrations are measured along two orthogonal directions per each plane and the vector of the additional vibrations is organized as follows:

$$\mathbf{\Xi} = \left\{ \xi_V^{(1)}(\Omega_1) \quad \xi_H^{(1)}(\Omega_1) \quad \cdots \quad \xi_V^{(l)}(\Omega_1) \quad \xi_H^{(l)}(\Omega_1) \quad \cdots \quad \xi_V^{(1)}(\Omega_{n_p}) \quad \xi_H^{(1)}(\Omega_{n_p}) \quad \cdots \quad \xi_V^{(l)}(\Omega_{n_p}) \quad (\xi_H^{(l)}\Omega_{n_p}) \right\}^{\mathrm{T}}, \tag{10}$$

where e.g. $\xi_V^{(1)}(\Omega_1)$ indicates the vertical vibration in the first measuring plane, evaluated at the rotating speed Ω_1.

These are the measured multiple outputs (MO) of the considered system. Then, introducing the admittance matrix of the system and dropping the subscript index n of the harmonic component order for simplicity, Eq. (5) becomes:

$$[\mathbf{Z}(\mathbf{\Omega})]\mathbf{X}(\mathbf{\Omega}) = \begin{bmatrix} \mathbf{Z}(\Omega_1) & 0 & 0 & 0 \\ 0 & \mathbf{Z}(\Omega_2) & 0 & 0 \\ \vdots & \vdots & \vdots & \vdots \\ 0 & 0 & 0 & \mathbf{Z}(\Omega_{n_p}) \end{bmatrix} \begin{Bmatrix} \mathbf{X}(\Omega_1) \\ \mathbf{X}(\Omega_2) \\ \vdots \\ \mathbf{X}(\Omega_{n_p}) \end{Bmatrix} = \begin{Bmatrix} \sum_{i=1}^{m} \mathbf{F}_f^{(i)}(\Omega_1) \\ \sum_{i=1}^{m} \mathbf{F}_f^{(i)}(\Omega_2) \\ \vdots \\ \sum_{i=1}^{m} \mathbf{F}_f^{(i)}(\Omega_{n_p}) \end{Bmatrix} = \mathbf{F}_f(\mathbf{\Omega}). \tag{11}$$

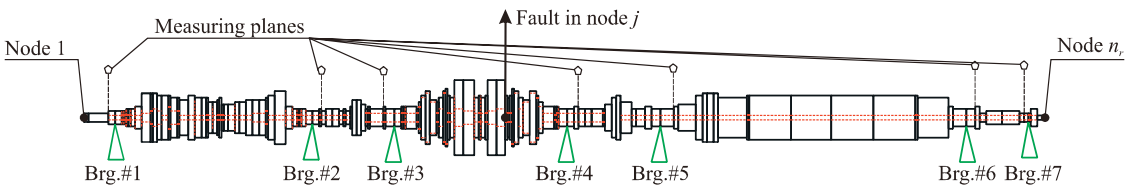

Fig. 17. General rotor model, location of the measuring planes and of a fault in a general node j.

If the rotor model has n_r nodes and the support structure is represented by means of a foundation with k_m dofs, the dofs of the fully assembled model are $(4n_r+k_m)$, while only $2l$ dofs are measured per each rotating speed. The admittance matrix $[\mathbf{Z}(\mathbf{\Omega})]$ has order $((4n_r+k_m)n_p \times (4n_r+k_m)n_p)$.

The equivalent excitation system, for each one of the m faults considered, is repeated for all the rotating speeds so that the fault vector is of order $((4n_r+k_m)n_p)\times m$; taking into account that in this case the unbalance is considered, in order to eliminate the dependence on the rotating speed square that appears in Eq. (8), it is convenient to insert Ω_j^2 in the localization vector of each rotating speed. Therefore, in the first node, the localization vector of the kth fault for the jth rotating speed is

$$\left\{\underline{\mathbf{L}}^{(k),(j)}\right\} = \Omega_j^2 \left\{ \underbrace{1 \quad 0 \quad i \quad 0}_{\text{1st node}} \quad \underbrace{0 \quad 0 \quad 0 \quad 0}_{\text{2nd node}} \quad \vdots \quad \underbrace{0 \quad 0 \quad 0 \quad 0}_{n_r\text{th node}} \quad \underbrace{0 \quad \ldots \quad 0}_{k_m \text{ dofs}} \right\}^{\mathrm{T}} \tag{12}$$

and for all the n_p rotating speeds:

$$\mathbf{L}^{(k)} = \left\{ \left\{\underline{\mathbf{L}}^{(k),(1)}\right\} \quad \cdots \quad \left\{\underline{\mathbf{L}}^{(k),(n_p)}\right\} \right\}^{\mathrm{T}}. \tag{13}$$

Since the faults have to be identified not only in their severity but also in their position, the identification procedure starts by assuming their positions as known and then identifies the corresponding amplitudes and phases. All the subsequent permutations of fault number and position have to be evaluated, unless the research of the faults is limited inside a specified interval of nodes. The permutations ${}_{n_r}P_m$ are indicated by the subscript so that (1, 5, …) means that the first excitation is applied in node 1, the second in node 5, etc.

These iterations are implemented in a loop. In the first step of the loop, all the equivalent excitations are supposed to be in the first node.

The effect on the measured dofs, due to all the exciting systems applied to the first node on the model and assumed to have unitary value ($\theta^{(k)}=1,\ \forall k$) is the vector $[\mathbf{Y}_{(1,\ldots,1)}]$ of order $(2ln_p \times m)$. Following the statistical nomenclature, $[\mathbf{Y}_{(1,\ldots,1)}]$ is the *model* matrix [20]. The kth column of the vector corresponds to the effect of the kth generalized force. The calculation of $[\mathbf{Y}_{(1,\ldots,1)}]$ is done first by substituting Eq. (13) in the right-hand side of Eq. (11), and inverting matrix $[\mathbf{Z}(\mathbf{\Omega})]$, obtaining the matrix $[\mathbf{H}(\mathbf{\Omega})]$

$$\mathbf{X} = [\mathbf{Z}(\mathbf{\Omega})]^{-1}\mathbf{L}(\mathbf{\Omega}) = [\mathbf{H}(\mathbf{\Omega})]\mathbf{L}(\mathbf{\Omega}). \tag{14}$$

Then, the vibrations of the dofs that are measured are separated from all the dofs of the system, by considering only the rows of $[\mathbf{H}(\mathbf{\Omega})]$ corresponding to the measured dofs. The partitioned matrix $[\underset{\sim}{\mathbf{H}}(\mathbf{\Omega})]$ is of order $(2ln_p \times (4n_r+k_m)n_p)$ and results:

$$[\mathbf{Y}_{(1,\ldots,1)}] = [\underset{\sim}{\mathbf{H}}(\mathbf{\Omega})]\left[\mathbf{L}^{(1)} \quad \vdots \quad \mathbf{L}^{(m)}\right]. \tag{15}$$

Now the array $\boldsymbol{\theta}$, which is of order $(m\times 1)$, of the complex values $\theta^{(i)}$ (i.e. the modules and phases) of the equivalent excitation systems applied to the first node that fits best the experimental data $\mathbf{\Xi}$, which is of the order $(2ln_p \times 1)$, has to be estimated. Under a statistical point of view, a linear regression model is used, where $\boldsymbol{\theta}$ is the parameter vector to be estimated and $\mathbf{r}$ the residual vector:

$$\mathbf{\Xi} = [\mathbf{Y}_{(1,\ldots,1)}]\boldsymbol{\theta} + \mathbf{r} = [\mathbf{Y}_{(1,\ldots,1)}]\left\{\begin{array}{c}\theta^{(1)}\\ \vdots \\ \theta^{(m)}\end{array}\right\} + \mathbf{r}. \tag{16}$$

Note that Eq. (16) indicates a linear system also under a mechanical point of view, since the measured vibrations are caused by the superposition of the effects of all the excitation systems applied. The fitting of the regression model, i.e. the minimization of the error, can be done by means of different approaches and in previous studies weighted least squares have been used. Here, M-estimators are used and this requires some modifications to the model-based identification technique.

The implementation of M-estimate requires two nested loops in this case; hence it requires longer calculation time, but greatly increases the robustness and therefore the accuracy of the obtained results.

The external loop is relative to the localization of the fault and it is equal to that of the L_2 method. The inner loop is that of the IRLS algorithm (see Ref. [1], Section 4 and Refs. [21,22]):

1. The initial estimate of the amplitudes and phases of the excitation systems in the current node is selected using the results of least squares estimate.
2. At each iteration t, the errors $e_i^{(t)}$ and the associated weights $w_i^{(t)}$ are calculated from the previous iteration.
3. The new weighted least squares estimate at iteration t is

$$\widehat{\boldsymbol{\theta}}^{(t)}_{(1,\ldots,1)} = \left([\mathbf{Y}_{(1,\ldots,1)}]^{\mathrm{T}}[\mathbf{W}^{(t)}][\mathbf{Y}_{(1,\ldots,1)}]\right)^{-1}\left[\mathbf{Y}_{(1,\ldots,1)}\right]^{\mathrm{T}}\left[\mathbf{W}^{(t)}\right]\boldsymbol{\Xi}, \tag{17}$$

where

$$\mathbf{W}^{(t)} = \mathrm{diag}\left[w_i^{(t)}\right]. \tag{18}$$

Steps 2 and 3 are iterated until convergence of the values of $\widehat{\boldsymbol{\theta}}_{(1,\ldots,1)}$ is achieved upon a stated criterion. The inner loop is then ended and the *relative residual* between the experimental data and the system response due to the identified faults in the first rotor node is determined, first by obtaining the calculated response due to the identified faults in the first node:

$$\widehat{\boldsymbol{\Xi}}_{(1,\ldots,1)} = [\mathbf{Y}_{(1,\ldots,1)}]\widehat{\boldsymbol{\theta}}_{(1,\ldots,1)} \tag{19}$$

and

$$\widehat{\delta}_{r_{(1,\ldots,1)}} = \left(\frac{\left[\boldsymbol{\Xi} - \widehat{\boldsymbol{\Xi}}_{(1,\ldots,1)}\right]^{*\mathrm{T}}\left[\boldsymbol{\Xi} - \widehat{\boldsymbol{\Xi}}_{(1,\ldots,1)}\right]}{\boldsymbol{\Xi}^{*\mathrm{T}}\boldsymbol{\Xi}}\right)^{1/2}. \tag{20}$$

The procedure then continues with the external loop and is iterated for the permutations ${}_{n_r}P_m$ so that the set of $\widehat{\boldsymbol{\delta}}_r$ in the $\mathbb{R}^m$ space is built up. The minimum value of $\widehat{\boldsymbol{\delta}}_r$ indicates along the m dimensions the most probable location of the faults, the estimations of which are given by the corresponding values of $\widehat{\boldsymbol{\theta}}_{(s)}$. The research for the minimum value of the relative residual set is the same performed in the case of use of the least squares estimate, as shown in Refs. [2,9].

3.2. Experimental results

The test-rig employed is that of Department of Mechanical engineering of Politecnico di Milano (PdM). It has been described in detail in Ref. [17] while the model has been tuned as described in Ref. [2], even if the tuning is not perfect in some frequency range.

The horizontal rotor, see Fig. 18, is composed by two rigidly coupled steel shafts (the span is about 2 m and the mass 90 kg) supported by four elliptical journal bearings. The variable speed electrical motor can drive the rotor up to a maximum speed of 6000 rev/min, while the flexible steel foundation, which has several natural frequencies in the operating speed range of the rotor, has been modelled by modal representation.

Two X–Y proximity probes in each bearing measure the relative shaft displacements and two X–Y accelerometers on each bearing housing measure its vibrations, therefore the measuring planes coincide with the bearings (Fig. 19). The absolute vibration of the shaft is calculated by adding the relative displacement measured by the proximity probes to the absolute bearing housing displacement, which is obtained integrating twice the acceleration measured by the accelerometers. A run-down test was performed in order to store reference vibration data.

Two known unbalances are applied on both shafts of the test-rig in the balancing planes corresponding to the nodes 9 (unbalance on the short shaft) and 35 (unbalance on the long shaft) in the finite beam model. The amplitude and the phase of both unbalances are the same and equal to 3.6e−4 kg m and -90°. Using the stored reference vibrations, the additional vibrations are obtained in the speed range 504–3001 rev/min. Two

Fig. 18. PdM test-rig.

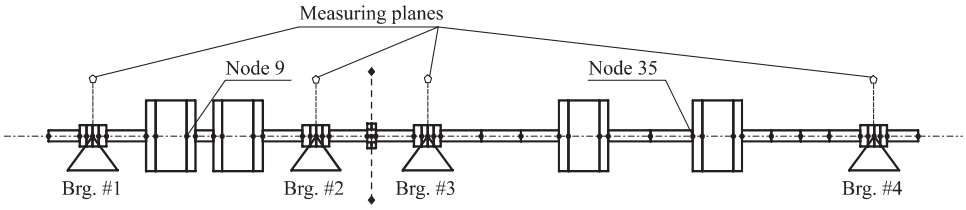

Fig. 19. Rotor model of the PdM test-rig.

unbalances being simultaneously identified, the relative residuals are calculated for the permutations ${}_{n_r}P_2$ and their set is in $\mathbb{R}^2$. Since the two faults are of the same kind, the residual surface representing the residual set is symmetric as shown in Fig. 20 (and therefore two minima are present).

Anyway, it is not easy to immediately identify the minimum in the surface, in case of use of both L_2 and Huber's M-estimate. Therefore a different representation of the surface is used, called *residual map*. In this representation, a colour code represents the value of the residual and vertical and horizontal axes corresponding to the rotor nodes. Using the residual map, the residuals are plotted in Fig. 21 for the L_2-estimate and in Fig. 22 for the M-estimate. The two darkest areas indicate the position of the two faults. It is possible to see that the M-estimate locates exactly the fault position, whilst the L_2-estimate does not. The complete results are summarized in Table 2. Also in this case, the M-estimate achieves a greater accuracy than the L_2-estimate, with regard not only to the fault positions but also to amplitudes and phases of the unbalances.

It is also interesting to note that, even if the stop condition of the IRLS algorithm is quite restricting, being the same of Eq. (4), the convergence of the estimated values of the two faults in correspondence of the minimum value of the $\boldsymbol{\delta}_r$ occurs before the maximum allowed number of iterations (see Fig. 23).

The comparison between the experimental measurements and the simulated results with the identified fault parameters is shown in Figs. 24–27 for bearings #1 and #3 only, along with the values of the weights in the last iteration as a function of the rotating speed, i.e. practically to the experimental observation reverse order. Since in this case the measurements were carefully made, a low weight indicates that the model fitting to the data is not good at this rotating speed.

This could be caused for instance by the calculation of the linearized dynamic stiffness coefficients that could not match exactly the journal bearing behaviour in all the considered speed range of the run-down, or by the presence of phenomena related to the supporting structure that have not been modelled or taken into account. In Figs. 24–27, it is possible to observe that generally low weights are attributed to the measurements corresponding to the critical speeds of the rotor. In these cases, the rotor orbits inside the bearings can become

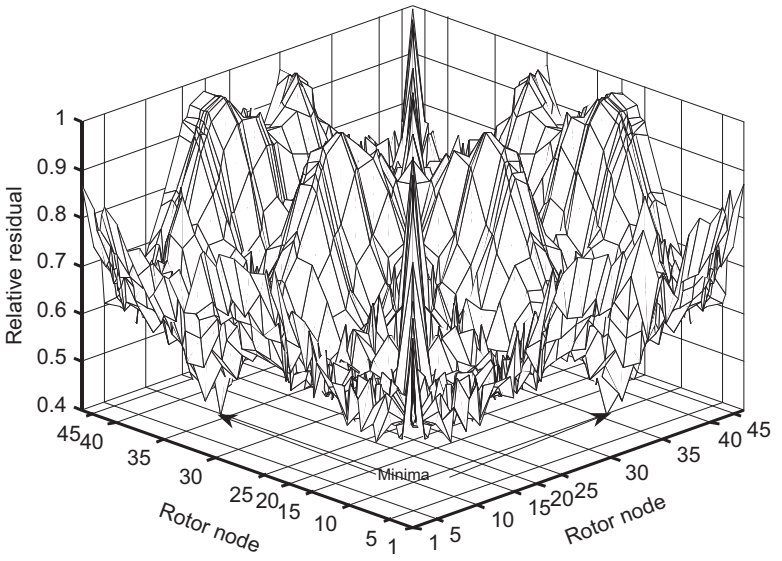

Fig. 20. Representation of the relative residual set for Huber's M-estimate.

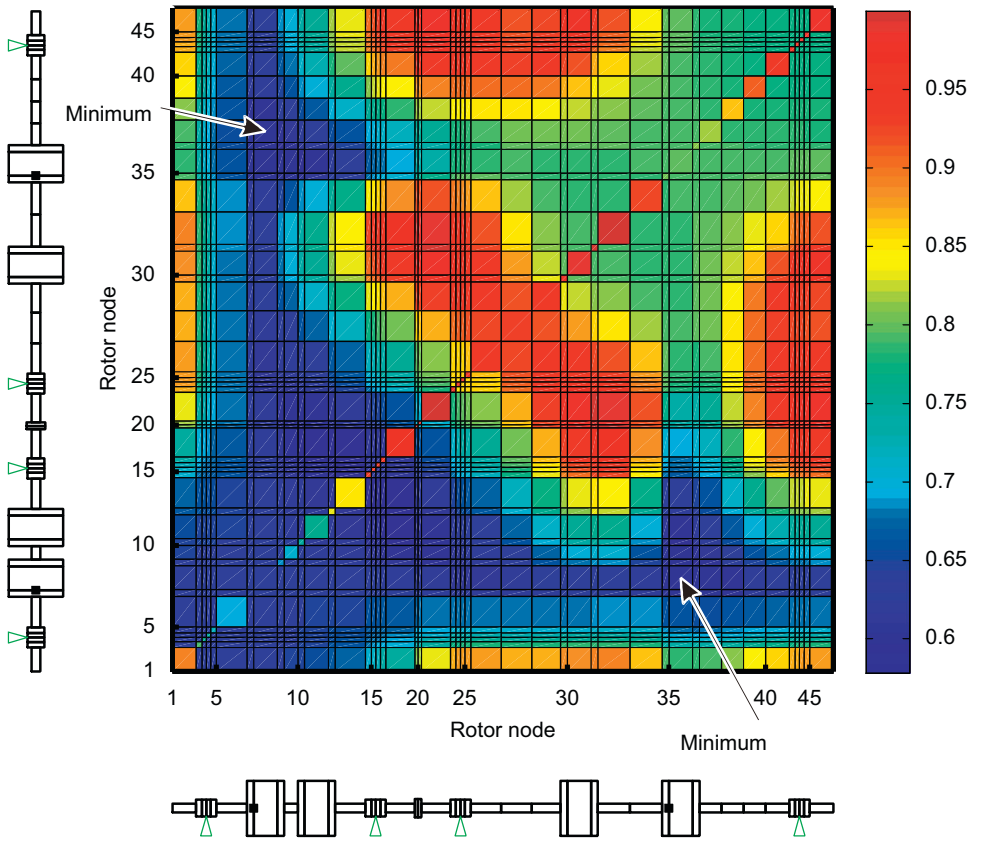

Fig. 21. Residual map for the L_2-estimate.

relatively large with respect to the clearances; some nonlinear effects can occur and the linearization of the oil-film forces cannot take into account all the phenomena.

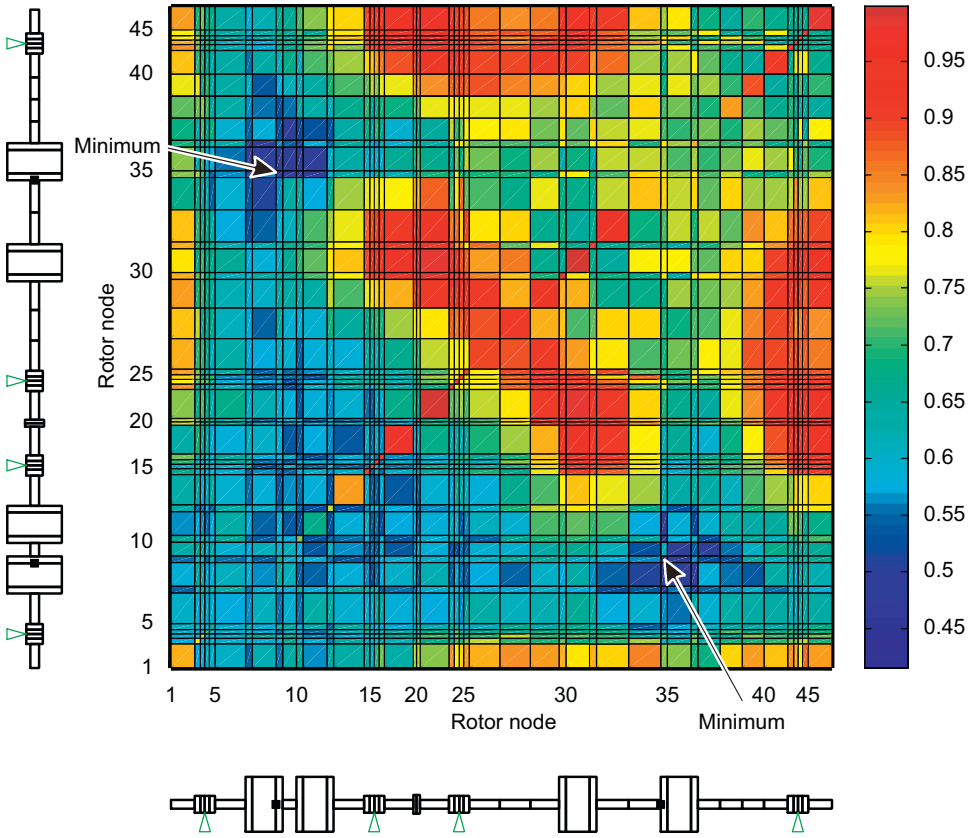

Fig. 22. Residual map for Huber's M-estimate.

Table 2
Results of two simultaneous unbalance identification in a rotor test-rig

	Nodes	Δl (m)	Amplitude (kg m)	Δmr (kg m)	Phase	$\Delta\varphi$ (deg.)	Rel. residual
Actual	9		3.60 e−4		−90°		
	35		3.60 e−4		−90°		
L_2-estimate	8	−0.07 (−3.59%)	4.22 e−4	0.62e−4 (17.22%)	−93.21°	−3.21	0.578
	36	0.02 (1.03%)	3.82 e−4	0.22e−4 (6.11%)	−102.52°	−12.52	
M-estimate (Huber)	9	0.00 (0.00%)	3.99 e−4	0.39e−4 (10.83%)	−91.23°	−1.23	0.415
	35	0.00 (0.00%)	3.55 e−4	−0.05e−4 (−1.39%)	−93.07°	−3.07	

The piece of information given by the weight values can be useful to decide in which frequency range a further model tuning could be performed. Comments are similar for the results in the bearings not shown.

4. Experimental results for a SIMO system: unbalance identification in a 320 MW steam turbo-generator

The proposed technique is applied to the identification of the unbalance in a real steam turbo-generator of a power plant. In this case, besides the accuracy of the identification, it is interesting to show that the capability of the M-estimator technique to perform the auto-rational-weighting of the data allows a successful identification without an expert's knowledge.

The considered machine and the experimental data have already been analysed in detail in a previous paper [18]. In that paper it has been shown that the model-based identification in the frequency domain for the rotor

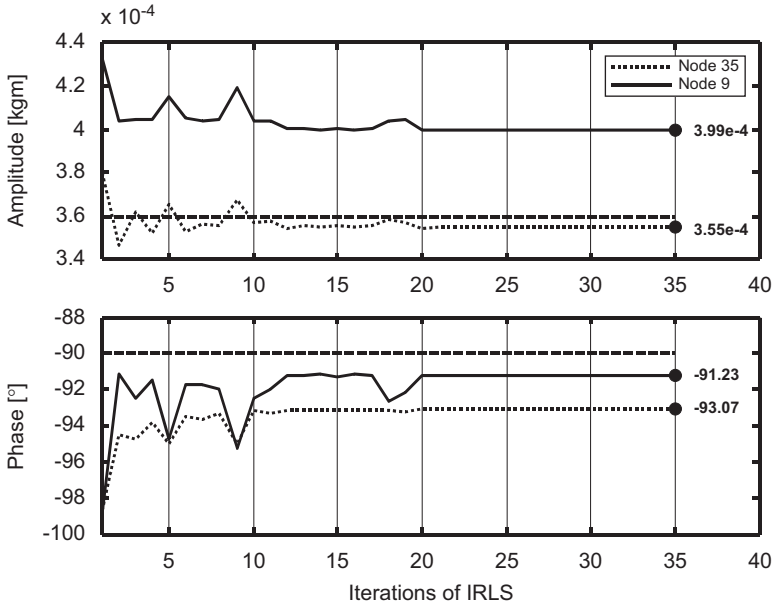

Fig. 23. Convergence of estimated parameters during IRLS iterations when the unbalances are located in nodes 9 and 35.

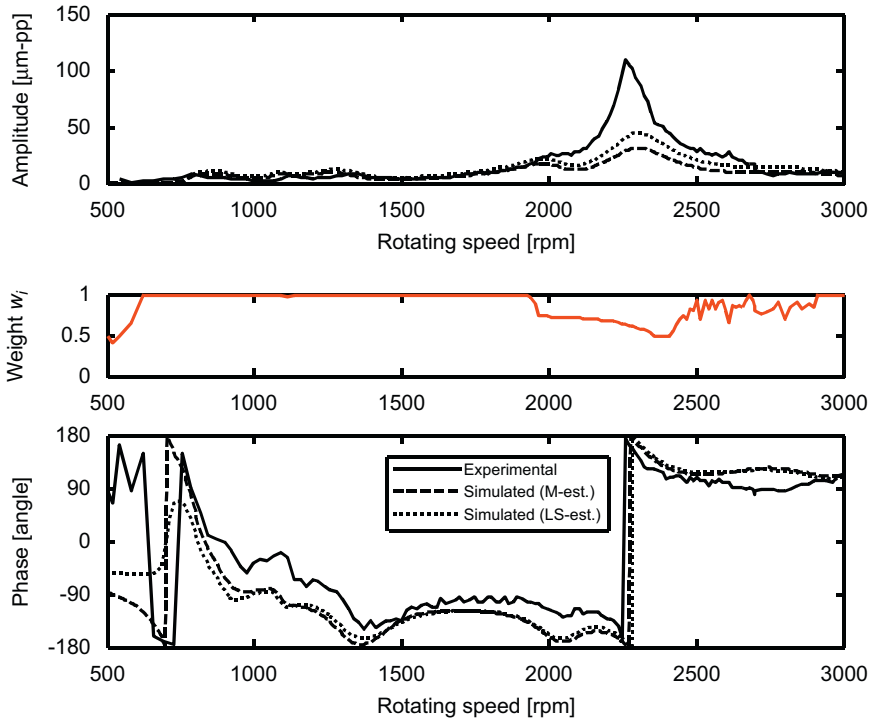

Fig. 24. Experimental, simulated vibrations with LS and M-estimate and vibration weights in the last step of the ILRS loop, brg. #1, vertical direction.

system obtained good results in identifying the unbalance of the machine, but that the best performances were obtained when weighted least squares were used. The attribution of the weights was made by expert's selection on the basis of the consideration that the accuracy of the machine model was higher in certain rotating speed

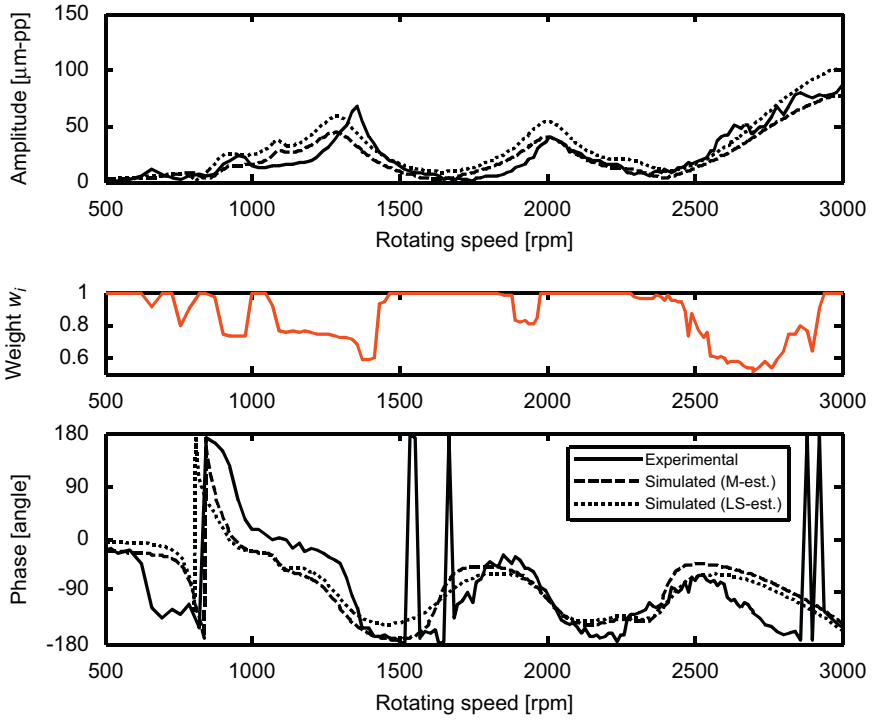

Fig. 25. Experimental, simulated vibrations with the LS- and M-estimates and vibrations weights in the last step of the ILRS loop, brg. #1, horizontal direction.

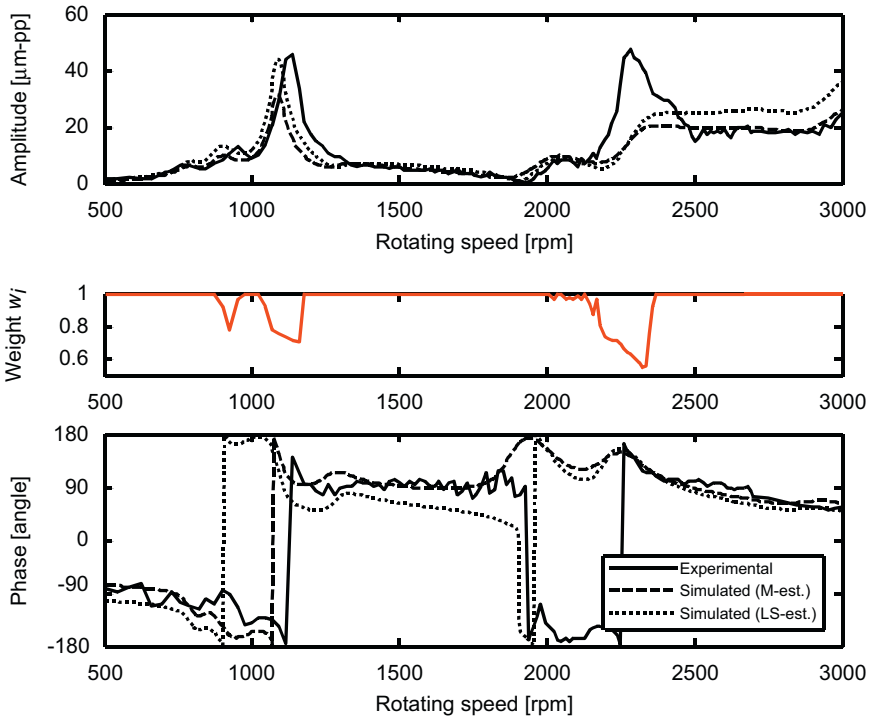

Fig. 26. Experimental, simulated vibrations with the LS- and M-estimates and vibration weights in the last step of the ILRS loop, brg. #3, vertical direction.

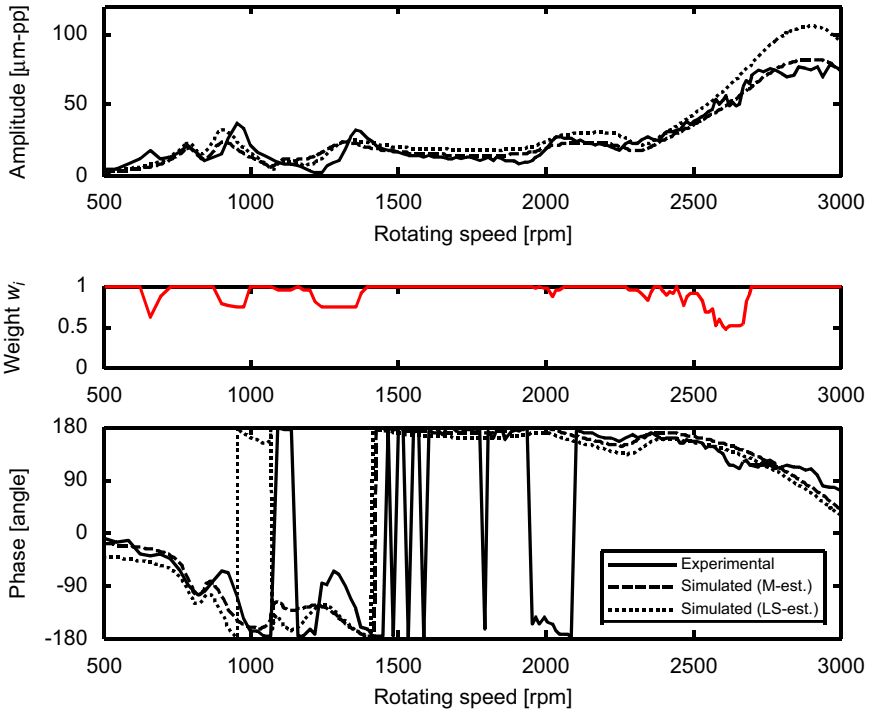

Fig. 27. Experimental, simulated vibrations with the LS- and M-estimates and vibration weights in the last step of the ILRS loop, brg. #3, horizontal direction.

ranges or that data from some measuring planes were more important. Actually the worst results were obtained when all the available additional vibration data (i.e. corresponding to each one of the rotating speed of run-down considered) were used and without weighting any measuring plane. However, this reflects actually the approach of a non-expert like a power plant operator of the control room. Now the same "blind" strategy is used along with the M-estimate.

The considered machine is a 320 MW fossil fuel steam turbine, the model of which has been already shown in Fig. 17. The details about the model assembling are reported in Ref. [18] so as the considerations about the linear behaviour of the machine. The experimental data used to obtain the additional vibrations are related to a run-down before and after a machine balancing. This way it is possible to know exactly the excitation position, amplitude and phase. Care was taken in order to choose two run-downs in similar thermal conditions. The balancing mass was on the first balancing plane of the generator that corresponds to the coupling face between the low-pressure turbine and the generator towards the last one (between bearing #4 and #5 in Fig. 17). The corresponding node of the model is 132. The overall amplitude of the balancing was of 0.256 kg m with a phase of -22.5° with respect to the key-phasor. Close to each lubricated journal bearing (the vertical dotted lines in Fig. 17) the shaft vibrations relative to the bearing housing were measured by a couple of X–Y proximity probes while the absolute vibrations of the supports were measured by a couple of X–Y velocimeters. Examples of the additional vibrations, i.e. the difference between balanced and unbalanced conditions, are shown in Fig. 28 for the measuring station close to bearing #4. Being only one excitation to be identified, the system is a SIMO.

The identification method is the same as used in Section 3.1, considering that $m = 1$ and therefore the relative residual set (for both the L_2 and M-estimate) are in the $\mathbb{R}$ space. The plot of the relative residual as a function of the rotor nodes or their axial position allows the minimum to easily indicate the excitation position along the rotor. Huber's M-estimator is used for the comparison. The two residual sets are shown in Fig. 29 and have different minima. Using the L_2-estimate, the unbalance position is node 134, whereas it is node 132, i.e. the exact position, for the M-estimate.

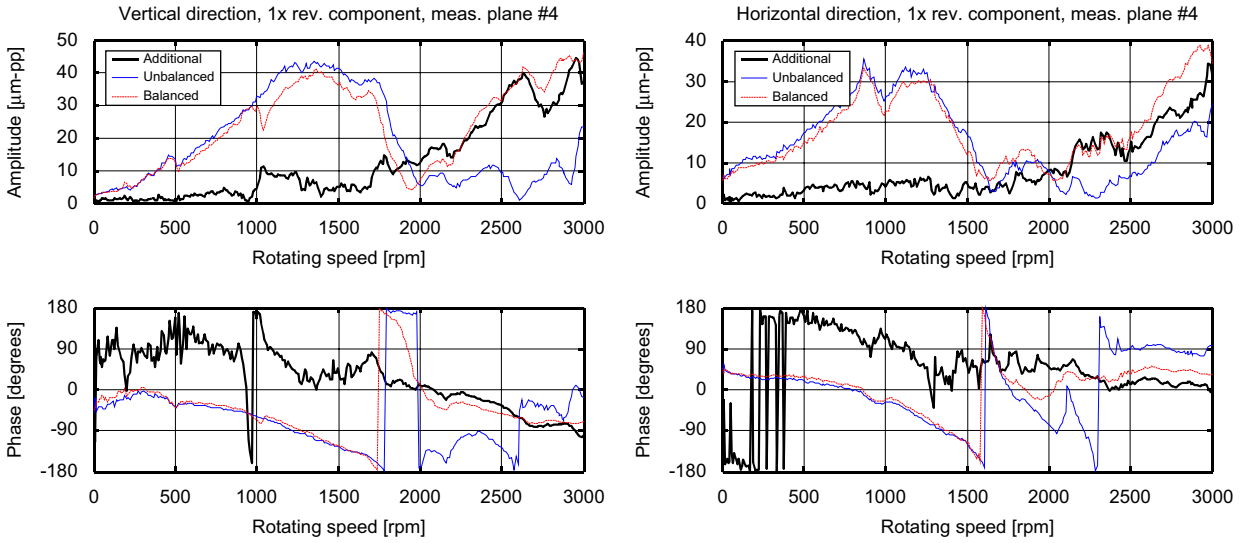

Fig. 28. 1× rev. vibrations in measuring plane #4. Thin line: absolute vibrations before balancing; dashed line: absolute vibrations after balancing; thick line: additional vibrations.

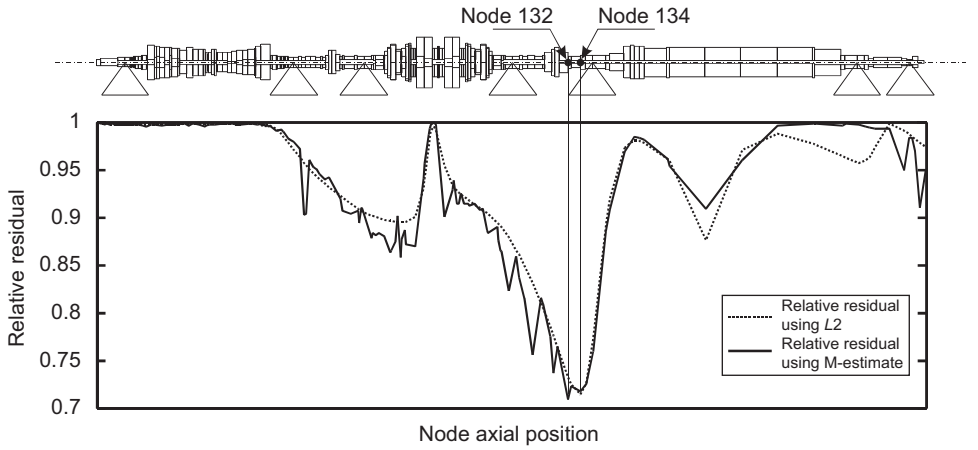

Fig. 29. Plot of the relative residual, calculated with L_2 and Huber's M-estimate, as a function of the node axial position along the rotor.

Table 3
Results of unbalance identification in a 320 MW steam turbo-generator

	Node	Δl (m)	Module [kg m]	Δmr (kg m)	Phase	$\Delta\varphi$ (deg.)	Rel. residual
Actual	132		0.256		−22.5°		
L_2-estimate	134	0.40 (1.40%)	0.186	−0.070 (−27.34%)	−18.6°	3.9	0.715
M-estimate (Huber)	132	0.00 (0.00%)	0.213	−0.043 (−16.80%)	−20.7°	1.8	0.709

The complete results are shown in Table 3. Obviously amplitude and phase obtained by the L_2-estimate are coincident with those obtained in Ref. [18]. The use of the M-estimate allows the exact position to be found out, without expert's selection of weights and in an automatic way, and also the accuracy in module and phase estimate is remarkable, especially considering the on-field case of a real rotating machine. In the node in which

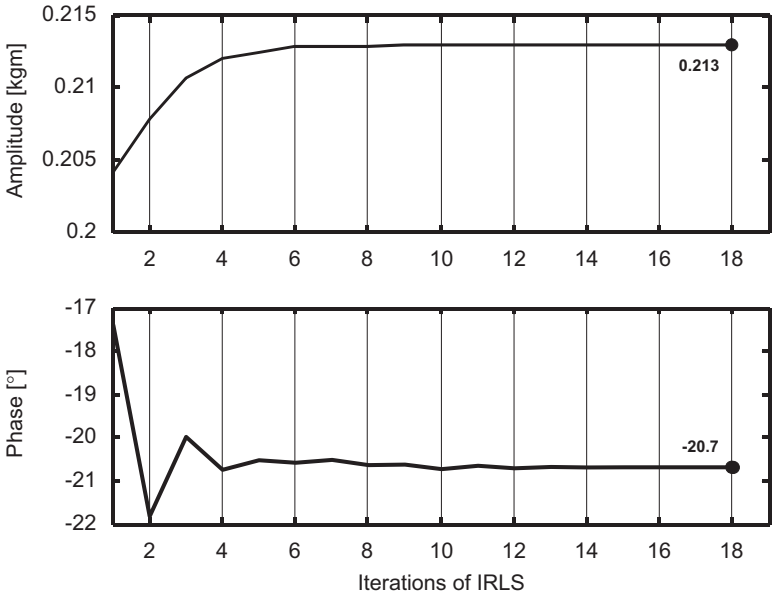

Fig. 30. Convergence of estimated parameters during IRLS iterations when the unbalances are located in node 132.

the unbalance is localized, the ILRS algorithm converges in only 18 iterations (the stop condition is that of Eq. (4)), see Fig. 30. Note that the values at the first iteration do not correspond to those of L_2 in Table 3, the nodes being different.

5. Conclusions

In this second part of the study, the performances of the M-estimate in order to increase the robustness of excitation identification in mechanical systems are evaluated on some SIMO and MIMO experimental cases. Two of them are related to test-rigs, whilst the third is a real machine. In all the proposed cases, the M-estimate allows accurate identification of the excitations, in terms of not only their magnitudes and phases, but also of their positions when pertinent.

The remarkable accuracy in the identification is obtained in an automatic way, i.e. the IRLS algorithm does not require any kind of pre-emptive expert's analysis of the data or attribution of weights. On the contrary this is often practically necessary if weighted least squares estimate is used, in order to obtain successful results. The IRLS algorithm is autonomously able to weight the data when the fitting between the experimental data and the physical model is not good. This implies that both noise on the experimental measure and some modelling errors are tolerated. In two of the examples presented in the paper, those related to rotor dynamics, this tolerance to modelling errors is effective to overcome possible lack of accuracy of machine model with regard to bearings and supporting structure. Moreover, the analysis of the weights given to a certain experimental value in certain conditions allows the model quality to be evaluated.

As regards the different types of M-estimators that have been proposed, the theoretical analysis and the numerical cases proposed in the first part of the paper have shown that only few of them are suitable. The experimental cases presented here confirm that only those having a unique solution are able to give a good estimation of the unknown parameters. In practice, Huber's M-estimator, which is the first historically introduced estimator, gives excellent results in all the cases under an engineering point of view.

References

[1] P. Pennacchi, Robust estimate of excitations in mechanical systems using M-estimators—theoretical background and numerical applications, *Journal of Sound and Vibration* 310 (4–5) (2008) 923–946.

[2] N. Bachschmid, P. Pennacchi, A. Vania, Identification of multiple faults in rotor systems, *Journal of Sound and Vibration* 254 (2) (2002) 327–366.
[3] T. Someya, *Journal-Bearing Databook*, Springer, Berlin, Heidelberg, Germany, 1989.
[4] D. Childs, *Turbomachinery Rotordynamics*, Wiley-Interscience, New York, USA, 1993.
[5] M.L. Adams, *Rotating Machinery Vibrations*, Marcel Dekker Inc., New York, USA, 2001.
[6] Z. Zhang, Parameter estimation techniques: a tutorial with application to conic fitting, *Image and Vision Computing* 15 (1997) 59–76.
[7] I. Mayes, J.E.T. Penny, Model based diagnostics of fault in rotating machines, *12th International Congress on Condition Monitoring and Diagnostic Engineering Management COMADEM 99*, Sunderland, July 1999, pp. 431–440.
[8] R. Platz, R. Markert, M. Seidler, Validation of online diagnostics of malfunctions in rotor systems, *Proceedings of IMechE—7th International Conference on Vibrations in Rotating Machinery*, University of Nottingham, UK, 12–14 September 2000, pp. 581–590.
[9] P. Pennacchi, N. Bachschmid, A. Vania, G.A. Zanetta, L. Gregori, Use of modal representation for the supporting structure in model based fault identification of large rotating machinery: part 1—theoretical remarks, *Mechanical Systems and Signal Processing* 20 (3) (2006) 662–681.
[10] M. Lalanne, G. Ferraris, *Rotordynamics Prediction in Engineering*, Wiley, Chichester, England, 1998.
[11] J. Kiciński, *Rotor Dynamics*, IFFM Publisher, Gdańsk, Poland, 2001.
[12] T. Konishi, P. Allaire, C. Untaroiu, Modal analysis of a large turbine-generator system with foundation effects, *IFToMM—6th International Conference on Rotor Dynamics*, Sydney, Australia, September–October 2002, pp. 846–853.
[13] N. Feng, E.J. Hahn, Numerical evaluation of an identification technique for flexibly supported rigid turbomachinery foundations, *IFToMM—6th International Conference on Rotor Dynamics*, Sydney, Australia, September–October 2002, pp. 854–861.
[14] M. Smart, M.I. Friswell, A.W. Lees, U. Prells, Estimating turbogenerator foundation parameters, *Proceedings of the Institution of Mechanical Engineers* 212 (Part C) (1998) 635–665.
[15] A.W. Lees, Improved machine vibration models, *IFToMM—6th International Conference on Rotor Dynamics*, Sydney, Australia, September–October 2002, pp. 235–242.
[16] Y. Kang, Y.-P. Chang, J.-W. Tsai, L.-H. Mu, Y.-F. Chang, An investigation in stiffness effects on dynamics of rotor-bearing-foundation systems, *Journal of Sound and Vibration* 231 (2) (2001) 343–374.
[17] N. Bachschmid, P. Pennacchi, E. Tanzi, A. Vania, Accuracy of modelling and identification of malfunctions in rotor systems: experimental results, *Journal of the Brazilian Society of Mechanical Sciences* XXII (3) (2000) 423–442.
[18] P. Pennacchi, N. Bachschmid, A. Vania, G.A. Zanetta, L. Gregori, Use of modal representation for the supporting structure in model based fault identification of large rotating machinery: part 2—application to a real machine, *Mechanical Systems and Signal Processing* 20 (3) (2006) 682–701.
[19] P. Pennacchi, N. Bachschmid, A. Vania, A model-based identification method of transverse cracks in rotating shafts suitable for industrial machines, *Mechanical Systems and Signal Processing* 20 (8) (2006) 2112–2147.
[20] P. Bickel, Robust Estimation, in: S. Kotz, N.L. Johnson, C.B. Read, N. Balakrishnan, B. Vidakovic (Eds.), *Encyclopedia of Statistical Sciences*, Vol. 8, Wiley, 1983, pp. 157–163.
[21] J. Fox, Robust regression, *An R and S-PLUS Companion to Applied Regression*, ⟨http://cran.r-project.org/⟩.
[22] D. Coleman, P. Holland, N. Kaden, V. Klema, S.C. Peters, A system of subroutines for iteratively reweighted least squares computations, *ACM Transactions of Mathematical Software* 6 (1980) 327–336.